Electrical Characteristics for Sn-Ag-Cu Solder Bump with Ti/Ni/Cu Under-Bump Metallization after Temperature Cycling Tests

T.I. SHIH,[1,2] Y.C. LIN,[1] J.G. DUH,[1,3] and TOM HSU[2]

1.—Department of Materials Science and Engineering, National Tsing Hua University, Hsinchu, Taiwan 300. 2.—United Microelectronics Corporation, Hsinchu, Taiwan 300. 3.—E-mail: jgd@mx.nthu.edu.tw

Lead-free solder bumps have been widely used in current flip-chip technology (FCT) due to environmental issues. Solder joints after temperature cycling tests were employed to investigate the interfacial reaction between the Ti/Ni/Cu under-bump metallization and Sn-Ag-Cu solders. The interfacial morphology and quantitative analysis of the intermetallic compounds (IMCs) were obtained by electron probe microanalysis (EPMA) and field emission electron probe microanalysis (FE-EPMA). Various types of IMCs such as $(Cu_{1-x},Ag_x)_6Sn_5$, $(Cu_{1-y},Ag_y)_3Sn$, and $(Ag_{1-z},Cu_z)_3Sn$ were observed. In addition to conventional I-V measurements by a special sample preparation technique, a scanning electron microscope (SEM) internal probing system was introduced to evaluate the electrical characteristics in the IMCs after various test conditions. The electrical data would be correlated to microstructural evolution due to the interfacial reaction between the solder and under-bump metallurgy (UBM). This study demonstrated the successful employment of an internal nanoprobing approach, which would help further understanding of the electrical behavior within an IMC layer in the solder/UBM assembly.

Key words: Lead free, solder, intermetallic compound (IMC)

INTRODUCTION

Flip-chip technology (FCT) developed since the 1960s[1] provides a great deal of beneficial advantages, including high input/output connections, low cost assembly, and high reliability. The Sn-Pb solder is widely used in today's electronic packaging. Nevertheless, because of the toxic effect of Pb on human beings and the environment, several Pb-free solders have been investigated to replace the Sn-Pb solder.[2–6] With the implementation of lead-free Sn-Ag-Cu solder in surface-mounted components such as flip-chip ball grid array (FC-BGA) packages, solder joint reliability of such electronic assemblies requires further research. Integrated circuit (IC) devices undergo thermal cycling during each power switch on/off cycle and thus stress becomes accelerated when exposed to different environments. Electronic assemblies usually have materials with large differences in the coefficient of thermal expansion (CTE) between the metallization layer and solder alloy.[7] Thus, solder joints are subjected to thermomechanical induced stresses, eventually leading to joint interface failures. As a result, thermal cycling and thermomechanical fatigue studies on lead-free solder joints are very important for understanding the reliability of lead-free solder joints.[8–10]

In the solder joint assembly after various heat treatments, intermetallic compounds (IMCs) were formed between the solder and under-bump metallurgy (UBM). The interfacial microstructure and IMC formation for different types of solders have been reported.[11–17] Nevertheless, data on the variation of electrical properties in solder joints were limited in the literature. The purpose of this work was to investigate the electrical characteristics of Sn-Ag-Cu solder bump with Ti/Ni/Cu UBM after the thermal cycle test. A conventional I-V measurement was conducted, incorporated with a novel design of a special sample section technique, to evaluate the resistance related to IMCs formed in the solder joint. In addition, a specially designed probing technique was developed to precisely evaluate the resistance in various parts of the solder joint. The electrical data corresponding to microstructural evolution at the interface of the solder joint were also discussed.

(Received March 9 2006; accepted May 3, 2006)

EXPERIMENTAL PROCEDURES

FC-BGA Specimens

Figure 1 shows the test specimen, i.e., flip-chip BGA with lead-free solder balls. The process for fabrication bumps used the stencil printing method. The ball diameter/pitch was 120 μm/200 μm. There were four perimeter rows with 1,500 solder balls and 17 solder balls at the center giving a total of 1,517 solder joints. The package type is high performance flip-chip ball grid array (HFC-BGA) with 1,517 solder balls (FC-BGA 1,517). The FC-BGA was soldered onto organic buildup using Sn-3.5Ag-0.5Cu lead-free solder. The detailed solder bump with Ti/Ni(V)/Cu UBM is shown in Fig. 2.

Temperature Cycle Conditions of Environmental Test

The temperature cycle test (TCT) has been widely used in current environment tests for flip-chip technology in industry. The flowchart for reliability test is shown in Fig. 3. The test specimens were conducted in an environmental test oven (Votsch VT7012 S2 System, Berlin, Germany). The dwelling time was 600 sec, 180 sec, and 600 sec at −65°C, 25°C, and 150°C, respectively. The temperature cycles of solder reflow ranged from 200 times to 500 times.

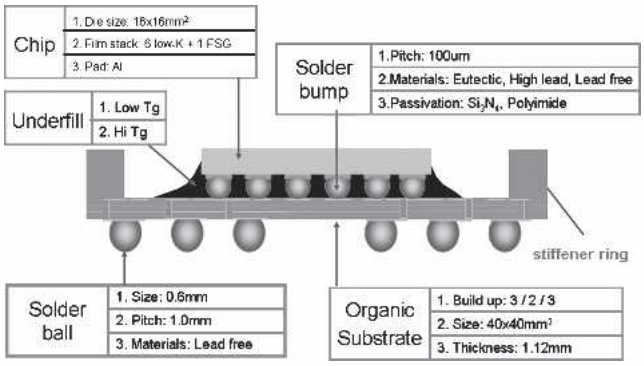

Fig. 1. FC-BGA 1,517 soldered onto organic buildup using Sn-3.5Ag-0.5Cu lead-free solder.

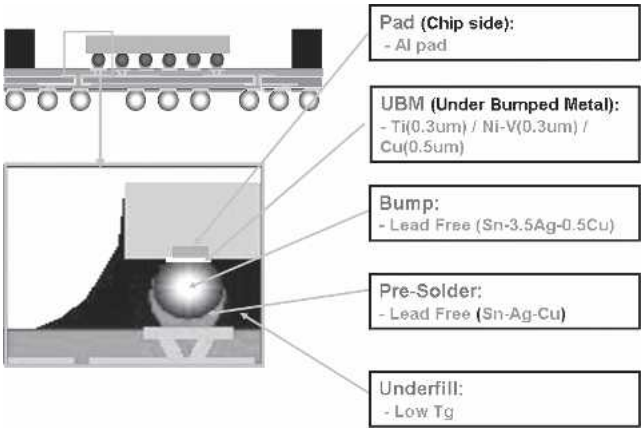

Fig. 2. The package type is HFC-BGA with 1,517 solder joints (FC-BGA 1,517). The FC-BGA was soldered onto organic buildup using Sn-3.5Ag-0.5Cu lead-free solder.

Sample Preparation of Cross-Sectional Observation for EPMA

For cross-sectional analysis, the sample was cold mounted in epoxy, sectioned by using a slow speed (50 rpm) diamond saw, ground, polished, and etched. For the top-view samples, the solder balls were etched directly with one part hydrochloric acid and nine parts methanol at room temperature.

Quantitative Analysis of Cross Section by EPMA

The morphologies of interfacial products between solders and UBM were observed with a field-emission scanning electron microscope (FE-SEM, JSM-6500F, JEOL, Tokyo). Compositions of phases in the solder joints and elemental distribution across the joint interface were quantitatively measured with an electron probe microanalyzer (EPMA, JXA-8800M, JEOL) with the aid of a ZAF program.[18]

Electrical Analysis by SEM Nanoprobing System

The SEM internal probing systems are positioning and testing tools for submicro- and nanoscale research, development application, and failure analysis. The SEM nanoprobing technique was developed for electric characteristics in the solder joint interface after different test conditions in this study.

For the electrical analysis, the sample was mounted in the steel holder, sectioned by using a slow speed (20 to 30 rpm) diamond saw, ground, and polished by slurry (HT-50) followed by a N_2 gun for drying. The solder balls were etched directly with buffered oxide etch solvent. The dwelling time was 2 to 3 sec for SEM observation. Deionized (DI) water was used to clean the residual acid of the

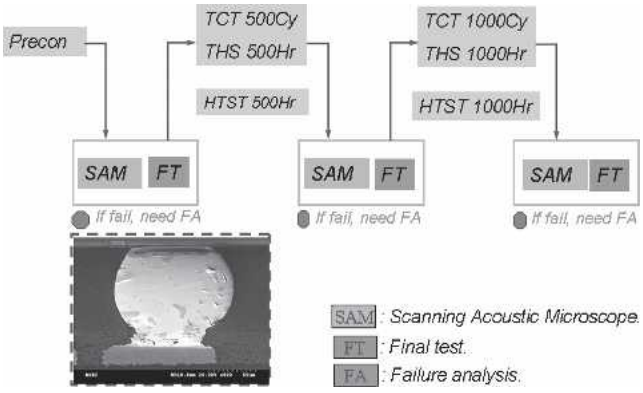

Fig. 3. The flowchart for the reliability test in industry.

sample surface followed by N_2 gun spray. The flowchart of the sample preparation of nanoprobing procedures is shown in Fig. 4.

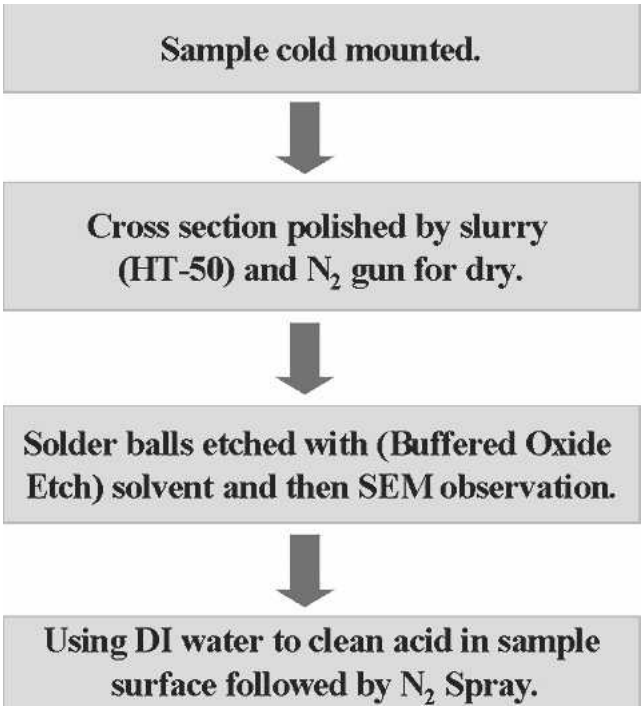

Fig. 4. The flowchart of the sample preparation of nanoprobing procedures.

The contact resistance of the IMC layer between the solder ball and UBM was measured with an SEM nanoprobing system (S100, Zyvex, Richardson, Texas) equipped with a cold field emission SEM (FEI-XL-30, Philips, Mahwah, NJ). There were three types of methods used in this study to conduct the electrical measurement. The first method is a conventional measurement via layer by layer with an electrical parameter analyzer (HP-4156C). The process flow of method I procedures is shown in Fig. 5. The diode I-V characteristics were measured between the solder ball and chip. The forward-bias diode I-V characteristics were first obtained and the slope (resistance) was then derived for the drain (or source) applied with a voltage from 1.0 to −1.0 V.

Both the second and third methods used an SEM nanoprobing system, in which method II was conducted in a fixed-distance measurement, while method III was done with two probes across different interfaces. The process flow of methods II and III are shown in Fig. 6.

RESULTS AND DISCUSSION

Before electrical measurement, it was better to first locate and then to characterize IMCs in the solder joint. To achieve a reliable quantitative analysis, a deliberative task in the EPMA operation was necessary.[16]

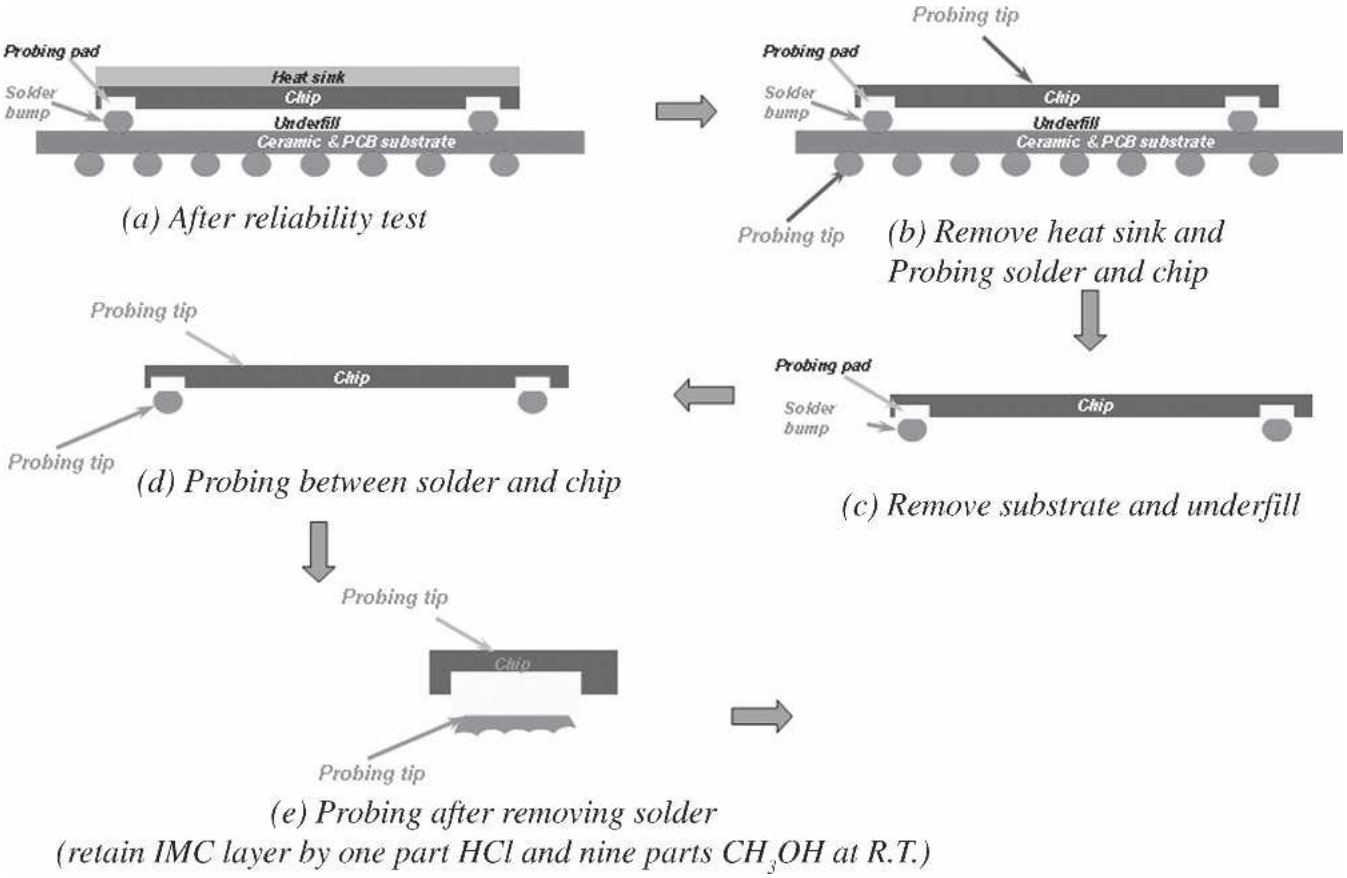

Fig. 5. The process flow of the electronic test in method I follows steps (a)–(e) to derive the electrical curve.

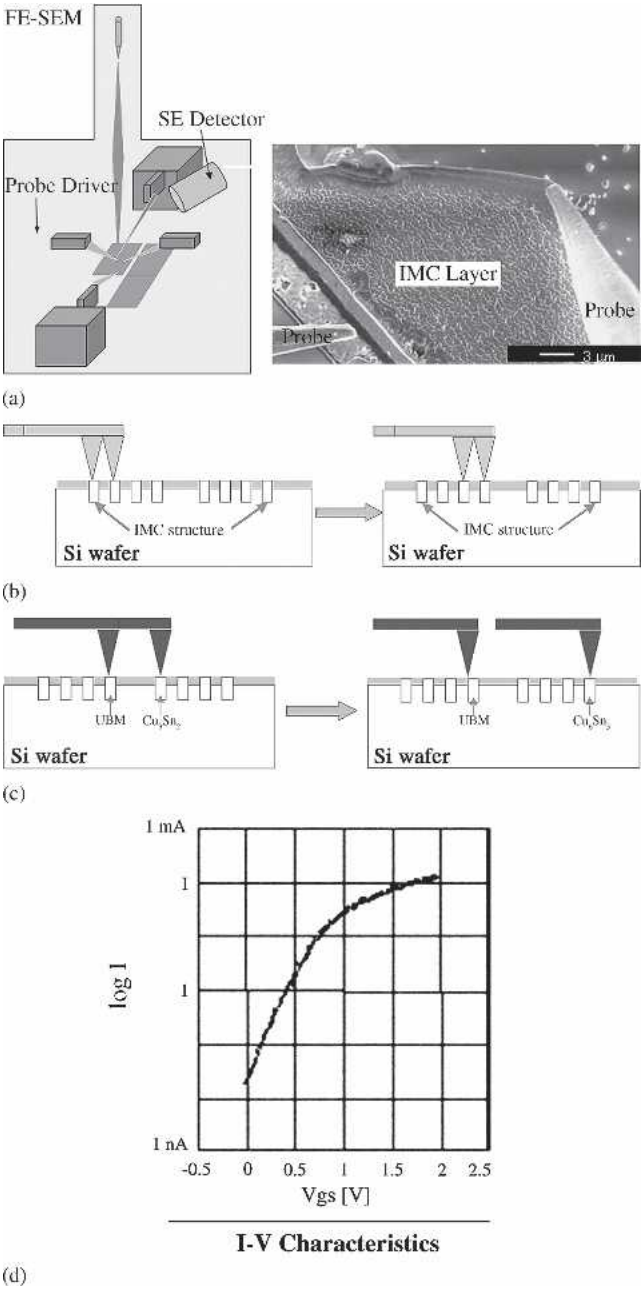

Fig. 6. (a)–(d) The process flow of nanoprobing procedures.

Interfacial Reaction between the Sn-3.5Ag0.5Cu Solder and Ti/Ni/Cu Under-Bump Metallization after TCTs

Figure 7 shows the cross-sectional images of interface between the Sn-3.5Ag-0.5Cu solder and Ti/Ni/Cu UBM after 200 cycles and 500 cycles during TCT. The interfacial morphology for 200 cycles of TCT was similar to that of 500 cycles. There was a major intermetallic compound formed near the interface, shown as the gray region in Fig. 7.

After quantitative analysis by FE-EPMA, the average composition of the interfacial product was 45.0at.%Sn-54.8at.%Cu-0.2at.%Ag in the Sn-3.5Ag0.5Cu solder joint after TCT 500 cycles. The reported compositions as listed in this study were the average of at least 10 measured points. The atomic ratio of (Cu + Ag) to Sn was 55.0:45, and closed to 6:5. Thus, the interfacial product is identified as $(Cu_{1-x},Ag_x)_6Sn_5$.

It should be pointed out there was another IMC formed adjacent to the UBM, which was the dark gray portion in Fig. 7. The FE-EPMA results revealed that the compositions for this smaller IMC were 74.4at%Cu-25.5%Sn-0.1at.%Ag. The ratio of Cu to Sn was 74.4:25.5 = 3:1, so that another Cu_3Sn IMC was observed.

Within the solder itself, there was a third IMC found, which was the precipitated particle, as indicated in Fig. 7b and d. The composition for this IMC, as indicated in Table I, was 71.0at.%Ag-28.2at.%Sn-0.8at.%Cu. The ratio of Ag to Sn was 71:28.2 ≒ 3:1. Thus, Ag_3Sn IMC was derived.

In consideration of the crystal structure of Cu, Sn, and Ag, because both Ag and Cu are face-centered cubic, there should exist some degree of mutual solubility for Ag and Cu in the IMC, as mentioned before. As a result, IMCs observed in the Sn-3.5Ag-0.5Cu/Cu/Ti/Ni solder joint could be denoted as $(Cu_{1-x},Ag_x)_6Sn_5$, $(Cu_{1-y},Ag_y)_3Sn$, and $(Ag_{1-z},Cu_z)_3Sn$.

Electrical Measurement between the Sn-3.5Ag0.5Cu Solder and Ti/Ni/Cu Under-Bump Metallization after TCTs

To assess both the IMC layer and the solder bump performance of ohmic contact to semiconductor chip, the contact resistance of the solder joint should be measured.[19] In this study, it was intended to precisely evaluate the resistance of IMCs, when exposed under the elevated temperature for a period of time.

Method I

In this study, method I was the electrical measurement done via the layer by layer feature, as indicated in Fig. 5. For statistical consideration, the measurement was carried out with the probing locations at five different and well-separated regions, i.e., (a) top left, (b) bottom left, (c) center, (d) top right, and (e) bottom right, as shown in Fig. 8. The reported data discussed below is the average for these five measurements.

Figures 9 and 10 indicate the I-V curves derived in the method I measurement for 200 and 500 cycles TCT, respectively. From the I-V characteristics, the corresponding resistance was calculated from the slope of the curve. Regarding Fig. 5, the resistance R_e measured in step (e) is

$$R_e = R_{IMC} + R_{chip} \quad (1)$$

where R_{IMC} and R_{chip} represent the resistance associated with the IMC and chip, respectively.

In the fabrication line, R_{chip} was a known parameter. The resistance data for the IMC can thus be obtained by

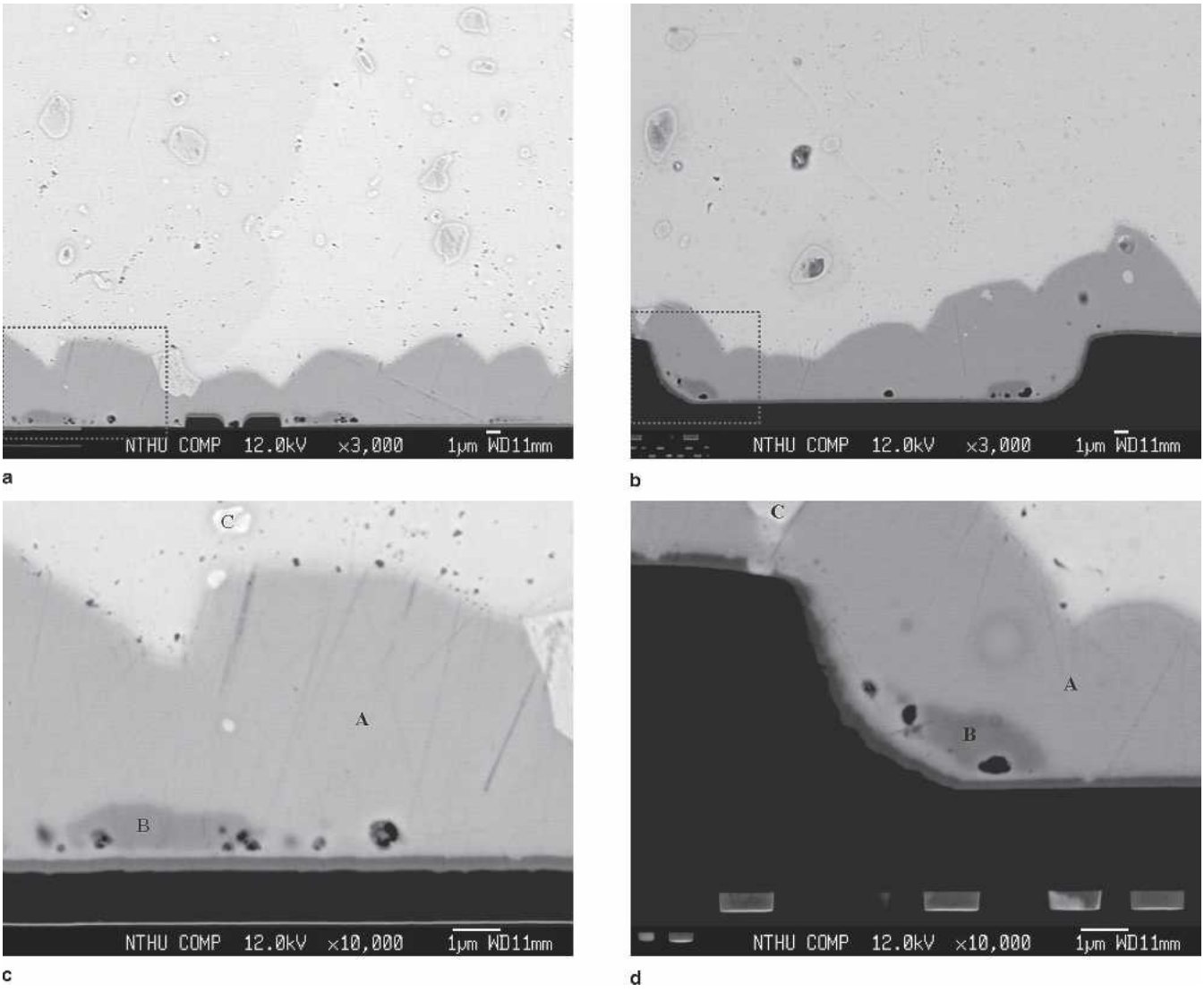

Fig. 7. Cross-sectional images of interfacial morphology in Sn-3.5Ag solder/Ni/Cu joints during TCT: (a) 200 cycles and (b) 500 cycles. (c) and (d) Enlarged images of (a) and (b), respectively.

$$R_{IMC} = R_e - R_{chip} \quad (2)$$

After 200 cycles TCT, the evaluated resistance for the IMC was 1,454 Ω, while that for the IMC after 500 cycles TCT was 1652 Ω. The resistance of IMCs in 200 TCT was a little smaller than that in 500 TCT, because the thickness of IMCs in 500 TCT was a little larger than that in 200 TCT, as indicated in Fig. 7.

The measured resistance of an IMC was related to its thickness after various thermal treatments. Nevertheless, the resistance as measured by method I after 200 and 500 cycles TCT was comparable in the range of 1,450 to 1,650, implying a reliable measurement technique for method I.

Method II

Method II in this study was conducted with probing in a fixed distance, i.e., 0.5 μm/step for each measurement. Figure 11 shows the SEM micrograph

Table I. Quantitative Analysis Results for Trace Points in Fig. 7 for the Sn-3.5Ag0.5Cu Solder Joints

(a) TCT-200 Cycle

Measurement Locations	Composition (At.%)			Phase
	Cu	Sn	Ag	
A	54.7	45.2	0.1	$(Cu_{1-x},Ag_x)_6Sn_5$
B	74.4	25.5	0.1	$(Cu_{1-y},Ag_y)_3Sn$
C	1.2	28.6	70.2	$(Ag_{1-z},Cu_z)_3Sn$

(b) TCT-500 Cycle

Measurement Locations	Composition (At.%)			Phase
	Cu	Sn	Ag	
A	54.8	45.0	0.2	$(Cu_{1-x},Ag_x)_6Sn_5$
B	74.4	25.3	0.3	$(Cu_{1-y},Ag_y)_3Sn$
C	0.8	28.2	71.0	$(Ag_{1-z},Cu_z)_3Sn$

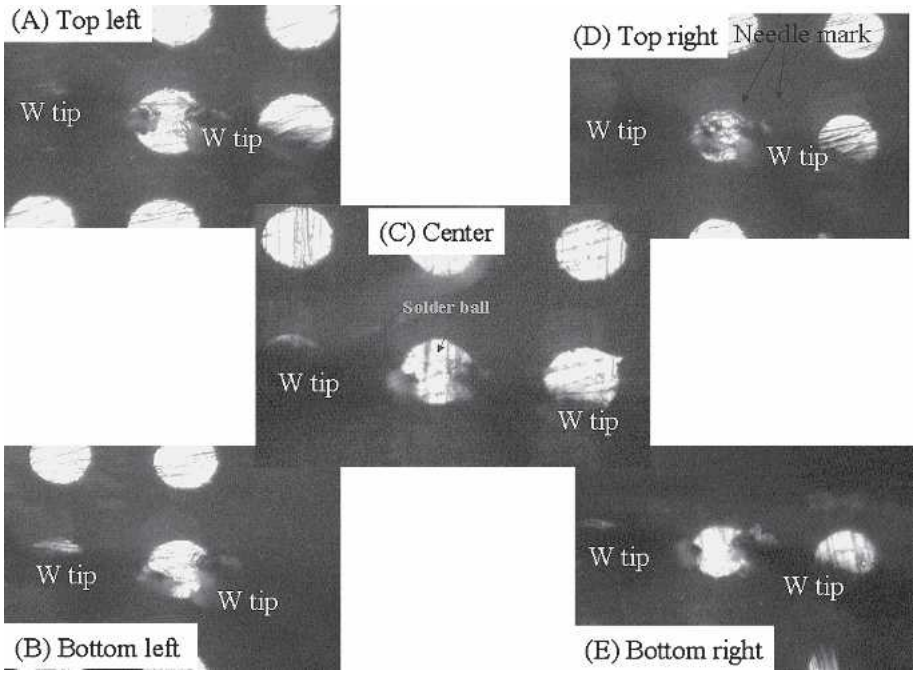

Fig. 8. The real probing location in method I showing (A)–(E) regions.

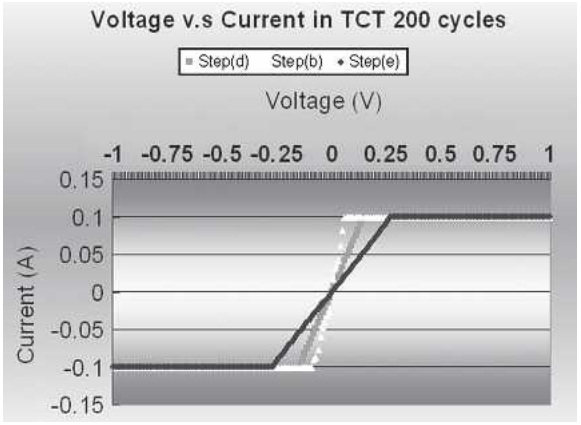

Fig. 9. I-V characteristics of TCT 200 cycles in method I.

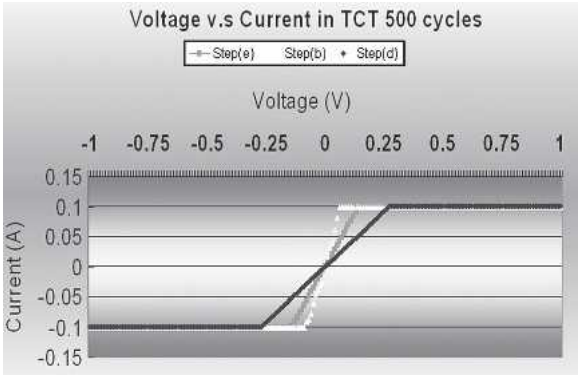

Fig. 10. I-V characteristics of TCT 500 cycles in method I.

when probing the TCT 200 sample. Figure 11a indicates the first point measurement from the UBM Ti/Cu to the IMC layer. Figure 11b shows the second measurement within the Cu_3Sn IMC, and Fig. 11c and d, the measurement within the Cu_6Sn_5 IMC.

The largest thickness of IMCs in sample TCT 500 was 6 μm, as shown in Fig. 7a, so there were totally 12 points of measurements in method II with the 0.5 μm/step. All of the measured resistances with respect to 12 points are listed in Table II. However, the IMC thickness in sample TCT 200 was a little smaller than 6 μm, so there were only 11 measurement points, as indicated in Table II.

In comparison to the data in Table II, it was revealed that the resistances for first point, i.e., UBM Ti/Cu, were 600 Ω and 589 Ω for TCT 200 and TCT 500, respectively. Similarly, the resistances for second point, i.e., UBM to the Cu_3Sn IMC, were 150 Ω and 145 Ω for TCT 200 and TCT 500, respectively. The consistent data after measurement were another indication of the reliable technique for method II. Again, all the measurements within the Cu_6Sn_5 layer at the 0.5 μm/step exhibit a resistance of 100 Ω for both TCT 200 and TCT 500. This is additional strong evidence for the measurement consistency in method II. As a result, the overall resistances of the total Cu_6Sn_5 layer in counting from point 1 to point 11 were 1,650 Ω and 1,634 Ω for TCT 200 and TCT 500, respectively.

Method III

In this study, method III was carried out by probing across different interfaces. Figure 12a indicates the probing across UBM Ti/Ni(V) and Cu, Fig. 12b is the probing between UBM(Ti) and thin Cu_6Sn_5 IMCs, and Fig. 12c shows the probing between UBM(Ti) and thick IMCs (Cu_6Sn_5). The fact that comparable resistance data were obtained for TCT 200 and TCT 500 under identical test conditions

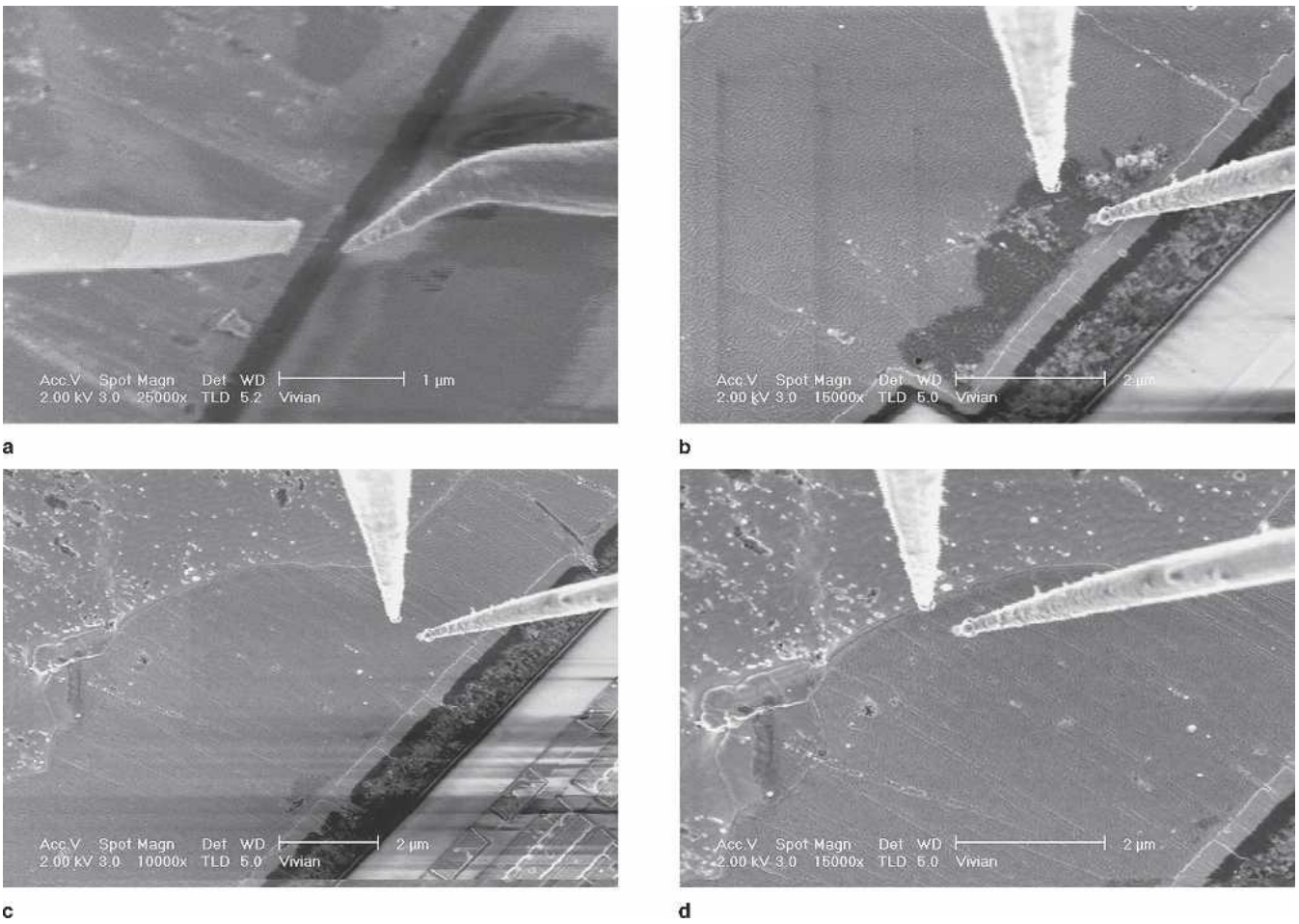

Fig. 11. SEM images when probing at a fixed distance for TCT 200 (method II) (0.5 μm/step): (a) first point from UBM (Ti)/Cu) to IMC layer, (b) second point within Cu_3Sn layer, (c) fourth point within Cu_6Sn_5 IMC layer, and (d) twelfth point within Cu_6Sn_5 IMC layer.

in Fig. 12a–c imply the reliable technique for method III.

In summary, the total resistances for the TCT 200 sample within the Cu_6Sn_5 IMC layer were 1,454 Ω, 1,650 Ω, and 1,672 Ω, as measured by methods I–III, respectively. For the TCT 500 sample, the resistances were 1,652 Ω, 1,634 Ω, and 1,652 Ω. All the data were nearly identical, and this provided strong evidence to support the measurement technique in methods I–III.

This research has demonstrated the successful employment of the internal nanoprobing technique along with the modified I-V curve method in the electrical measurement of the solder joint in the microelectronic package. Nanoprobing can be carried out at either fixed distances or across different interfaces, and it exhibits reliable data in the resistance measurement. This helps enable analysts to further appreciate the electrical behavior in the IMC and UBM layer. It is expected that the nanoprobing method will also exhibit the capability to measure straight sheet resistance in small areas (>40 nm^2) of the IMC layer. This technique will be equally valid for complicated back-end structures currently used in advanced very-large scale integration (VLSI) technologies.

CONCLUSIONS

- Interfacial microstructure and electrical characteristics between the Ti/Ni/Cu UBM and Sn-Ag-Cu solders after the temperature cycling test were investigated by the modified I-V and SEM nanoprobing technique.
- Two different measurement techniques were employed in the SEM internal probing system to evaluate the electric characteristics in the Cu_6Sn_5 IMCs after different test conditions for 200 and 500 cycles. The sheet resistance of the Cu_6Sn_5 IMCs was about 100 ohm in every 0.5-μm distance.
- The evaluated resistance for the Cu_6Sn_5 IMCs was nearly identical among the three different methods conducted in this study, indicating that a reliable test technique could be established. The electric data would be correlated to microstructural evolution due to the interfacial reaction between the solder and UBM.

ACKNOWLEDGEMENTS

The joint assembly preparation from United Microelectronics Corporation (UMC) is appreciated. Financial support from the National Science Council,

Table II. Summary of Resistance in IMCs and Solder Balls Measured by Various Methods for TCT 200 Cycle and TCT 500 Cycle Samples

Method	Probe Point	Probing Layer (Minimum Thickness of IMC = 2.85 μm, Maximum Thickness of IMC = 6.0 μm)	Distance (μm) (from UBM Start)	TCT-200 Resistance (Ohm)	TCT-500 Resistance (Ohm)
Method 1	Measure 1	IMC layer	0.5	1454	1652
Method 2	Measure 1	UBM (Ti) to UBM (Cu) layer	0.5	600	589
(fixed-distance)	Measure 2	IMC (Cu_3Sn) layer	1.0	150	145
	Measure 3	IMC (Cu_6Sn_5) layer	1.5	100	100
	Measure 4	IMC (Cu_6Sn_5) layer	2.0	100	100
	Measure 5	IMC (Cu_6Sn_5) layer	2.5	100	100
	Measure 6	IMC (Cu_6Sn_5) layer	3.0	100	100
	Measure 7	IMC (Cu_6Sn_5) layer	3.5	100	100
	Measure 8	IMC (Cu_6Sn_5) layer	4.0	100	100
	Measure 9	IMC (Cu_6Sn_5) layer	4.5	100	100
	Measure 10	IMC (Cu_6Sn_5) layer	5.0	100	100
	Measure 11	IMC (Cu_6Sn_5) layer	5.5	100	100
	Measure 12	IMC to solder ball	6.0	—	700
		Total layer (UBM + IMC)	6.0	1650	1634
Method 3	Measure 1	UBM (Ti) to UBM (Cu) layer	0.5	700	666
(various interface)	Measure 2	UBM (Cu) to IMC (Cu_3Sn)	1.0	150	150
	Measure 3	IMC (Cu_3Sn) to IMC (Cu_6Sn_5)	4.5	777	836
	Measure 4	IMC (Cu_6Sn_5) to Solder ball	6.0	—	850
		Total layer (UBM + IMC)	6.0	1627	1652

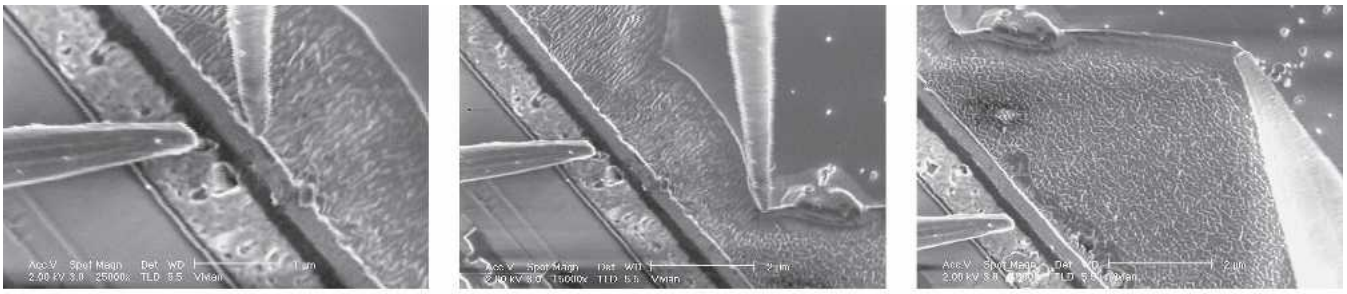

a b c

Fig. 12. SEM images when probing for TCT 200 across various interface measurements (method III): (a) probing UBM (Ti/Ni(V)/Cu), (b) probing between UBM (Ti) and thin IMCs (Cu_6Sn_5), and (c) probing between UBM (Ti) and thick IMCs (Cu_6Sn_5).

Taiwan, under Contract No. NSC-94-2216-E-007-016 is also acknowledged.

REFERENCES

1. L.F. Miller, *IBM J. Res. Dev.* 13, 239 (1969).
2. K.S. Bae and S.J. Kim, *J. Mater. Res.* 17, 743 (2002).
3. D.R. Frear, J.W. Jang, J.K. Lin, and C. Zang, *JOM* 53, 28 (2001).
4. B.L. Young, J.G. Duh, and B.S. Chiou, *J. Electron. Mater.* 30, 543 (2001).
5. M. McCormack, S. Jin, G.W. Kammlott, and H.S. Chen, *Appl. Phys. Lett.* 63, 15 (1993).
6. J.W. Jang, A.P. De Silva, J.K. Lin, and D.R. Frear, *J. Mater. Res.* 19, 1826 (2004).
7. H.W. Miao and J.G. Duh, *Mater. Chem. Phys.* 71, 255 (2001).
8. J.H.L. Pang, T.H. Low, B.S. Xiong, L.H. Xu, and C.C. Neo, *Thin Solid Films* 370, 462 (2004).
9. J.H.L. Pang, T.H. Low, B.S. Xiong, and F.X. Che, *Proc. IEEE, 2003 Electronics Packaging Technology Conf.* (Piscataway, NJ: IEEE, 2003), pp. 470–478.
10. F.A. Stam and E. Davitt, *Microelectron. Reliab.* 41, 1815 (2001).
11. S.K. Kang, R.S. Rai, and S. Purrshothaman, *J. Electron. Mater.* 25, 1113 (1996).
12. B.L. Young and J.G. Duh, *J. Electron. Mater.* 30, 878 (2001).
13. C.S. Huang, J.H. Yeh, B.L. Young, and J.G. Duh, *J. Electron. Mater.* 31, 1230 (2002).
14. J.W. Nah and K.W. Paik, *IEEE Trans. Compon. Packaging Technol.* 25, 32 (2002).
15. J.H. Lee, J.W. Park, D.H. Shin, and Y.S. Kim, *J. Electron. Mater.* 33, 28 (2004).
16. G.Y. Jang and J.G. Duh, *J. Electron. Mater.* 34, 68 (2005).
17. Y.C. Lin, J.G. Duh, and B.S. Chiou, *J. Electron. Mater.* 35, 7 (2006).
18. J.I. Goldstein, *Scanning Electron Microscopy and X-ray Microanalysis* (New York: Plenum Press, 1992), pp. 306–330.
19. G.K. Reeves and H.B. Harrison, *IEEE Electron Dev. Lett.* EDL-3, 111 (1982).